Science Advances
AAAS

Supplementary Materials for

Marine high temperature extremes amplify the impacts of climate change on fish and fisheries

William W. L. Cheung*, Thomas L. Frölicher, Vicky W. Y. Lam, Muhammed A. Oyinlola, Gabriel Reygondeau, U. Rashid Sumaila, Travis C. Tai, Lydia C. L. Teh, Colette C. C. Wabnitz

*Corresponding author. Email: w.cheung@oceans.ubc.ca

Published 1 October 2021, *Sci. Adv.* **7**, eabh0895 (2021)
DOI: 10.1126/sciadv.abh0895

This PDF file includes:

Supplementary methods

Modelling fisheries stock biomass and maximum catch potential

We used the Dynamic Bioclimate Envelope Model (DBEM) to simulate changes in distribution, abundance and catches of exploited marine fishes and invertebrates. The structure of the DBEM is described in (*59*) and we summarize pertinent aspects of the model here.

a. Current species distribution

The current distributions of commercially exploited species, representing the average pattern of relative abundance in recent decades (i.e., 1970-2000), were produced using an algorithm described in (*60*). The algorithm predicts the relative abundance of a species on a 0.5º latitude x 0.5º longitude grid based on the species' depth range, latitudinal range, known Food and Agriculture Organization statistical areas and polygons encompassing their known occurrence regions. The distributions were further refined by assigning habitat preferences to each species, such as affinity to shelf (inner, outer), estuaries, and coral reef habitats. The required habitat information was obtained from FishBase (www.fishbase.org) and SeaLifeBase (www.sealifebase.org), which contains key information on the distribution of the species in question, and on their known occurrence region. Catch data from the Sea Around Us project is not used in the algorithm to predict current species distribution.

b. Predicting future habitat suitability

We calculated an index of habitat suitability for each species (P) in each spatial cell i from temperature (bottom and surface temperature for demersal and pelagic species, respectively), bathymetry, specific habitats (coral reef, continental shelf, slope and seamounts), salinity (bottom and surface temperature for demersal and pelagic species, respectively) and sea ice with 30-year averages of outputs from 1971-2000 from GFDL ESM2M model. The multiple of these five components resulted in the overall habitat suitability:

$$P_i = P(T_i, TPP) \cdot P(Bathy_i, MinD, MaxD) \cdot P(Habitat_{i,j}, HAssoc) \cdot P(Salinity_i, SAssoc) \cdot P(Ice_i, IceP) \quad \text{(eq. S1)}$$

where *T* is seawater temperature, *Bathy* is bathymetry, *Habitat* is the proportion of area of the habitat type *j* relative to the total seawater area of the cell *i, Ice* is sea ice extent, and *Salinity* is the salinity class of cell *i* according to the Thalassic series (hyperhaline, metahaline, mixoeuhaline, polyhaline, mesophaline and oligohaline). For each species, *TPP* is temperature preference profile, *MinD* and *MaxD* are minimum and maximum depth limits, *HAssoc* is habitat association index, and *SAssoc* has a value of 1 or 0 indicating whether the species is or is not associated to the specific salinity classes, respectively, and *IceP* is association to sea ice for polar species.

Specifically, DBEM estimated the temperature preference profile (TPP) of each species by overlaying the estimated species distribution (*59*, *61*) with annual seawater temperature and calculated the area-corrected distribution of relative abundance across temperature for each year from 1971 to 2000, subsequently averaging annual temperature preference profiles (TPP). The TPP was calculated from the predicted average relative abundance (*Ri*) from the estimated current species distribution in temperature class *i* over the entire range:

$$TPP_i = \frac{R_i}{\sum R_i} \quad \text{(eq. S2a)}$$

$$R_i = \frac{Q_i}{A_i} \quad \text{(eq. S2b)}$$

where, Q_i and A_i are the sum of relative abundance and range area from spatial cells within temperature class *i*, respectively.

A species' distribution was also limited indirectly by depth. Thus, there were lower and upper limits of water depth (*minD* and *maxD,* respectively) outside of which a species does not occur*:*

$P(Bathy,minD,maxD) = 1$ if $Bathy \geq minD$ and $Bathy \leq maxD$ (eq. S3a)

$P(Bathy,minD,maxD) = 0$ if $Bathy < minD$ or $Bathy > maxD$ (eq. S3b)

However, marine species can survive in deeper waters than they currently occur to some extent. To reflect this, the model allows the species to move to areas where depth is twice the maximum depth limit. This assumption is to make sure that the species have sufficient scope to expand their depth range, while the extent of shift in depth range would be limited by other environmental variables that link to the species physiology and ecology (e.g., temperature, oxygen and food).

Each species was assigned an index of association (*HAssoc*) to one or more of the four habitat types: coral reefs, estuaries, seamounts and habitats that are none of the above. The index, scaled between 0 and 1, represents the relative density of a species in the particular habitat. It was assigned based on qualitative descriptions of the ecology of the species from FishBase or other publications and literature. Distribution of relative abundance was then adjusted based on the habitat-association index and the global distribution of each habitat:

$P(Habitat, HAssoc) = Habitat \cdot HAssoc$ (eq. S4)

Polar ecosystems, and the distributions of their associated species, are largely shaped by the dynamics of sea ice. In both the Arctic and around Antarctic, primary productivity close to sea ice is generally high (*80*). For instance, in the Antarctic, phytoplankton growth is enhanced by micronutrient delivery and stabilization of the water column associated with the influx of fresh and nutrient rich water from melting ice. This in turn forms the base of the foodweb, which supports fishes and mammals in polar ecosystems. Thus, polar fishes are generally distributed close to sea ice. It is therefore reasonable to assume that environmental preferences of polar species are partly dependent on distance from sea ice. To be consistent with the current species distributions, which represent annual averages, annual average sea ice extent was used. We calculated polar species' relative habitat suitability in relation to sea ice using similar algorithms as when calculating *TPP*. However, instead of seawater temperature, sea ice extent was used in eq. S2.

c. Modelling dispersal and movement of larvae and juvenile/adult

Movement and dispersal of adults and larvae were modelled through advection-diffusion-reaction equations for larvae and adult stages using equations 5a and 5b, respectively.

$$\frac{\partial A}{\partial t} = \frac{\partial}{\partial x}\left(D\frac{\partial A}{\partial x}\right) + \frac{\partial}{\partial y}\left(D\frac{\partial A}{\partial y}\right) - \frac{\partial}{\partial x}(u \cdot A) - \frac{\partial}{\partial y}(v \cdot A) - \lambda \cdot A \qquad \text{(eq. S5a)}$$

$$\frac{\partial A}{\partial t} = \frac{\partial}{\partial x}\left(D\frac{\partial A}{\partial x}\right) + \frac{\partial}{\partial y}\left(D\frac{\partial A}{\partial y}\right) + G \qquad \text{(eq. S5b)}$$

where A was abundance. Horizontal diffusion was characterized by a diffusion parameter D. The diffusion coefficient, expressed in $m^2\ s^{-1}$, is assumed to be a function of the length scale of the spatial grid: $D = (1.1 \times 10^{-4}) \cdot GR \cdot 1.33$ where GR is the minimum grid resolution. Pelagic larvae were assumed to be passively advected and diffused via ocean currents and associated mixing. Advection was characterized by two surface current velocity parameters (u, v) obtained from the GFDL Earth system model that described the east-west and north-south current movement across a distance between centers of neighboring cells in the east-west and north-south directions (x, y respectively). The duration of the pelagic larvae phase was predicted from an empirical equation as a function of sea surface temperature (*81*). The default larval mortality and larvae settlement rates are 0.85 $day^{-1}$and 0.2 day^{-1}, respectively. Sensitivity analysis suggests that the long-term (decadal) projection of DBEM is not sensitive to these two parameters. The instantaneous rate of larval mortality and settlement is represented by λ. Population growth (G) was modeled separately (see eq. S9). Colonization of new habitat (species invasion) is a result of either dispersal of larvae or movement of adults to the new habitat. Species turnover is partly dependent on species invasion.

For juvenile-adult stages, diffusion rate was dependent on habitat suitability (P) and a density-dependent factor (ρ) that was a function of the carrying capacity (Θ), abundance (A) and mean weight ($\underline{W}$) in the spatial cell i:

$$D_i = \frac{D_0 \cdot m}{1+e^{(\tau \cdot P_i \cdot \rho_i)}} \quad \text{(eq. S6)}$$

$$\rho_i = 1 - \frac{A_i}{(\theta_i / \underline{W}_i)} \quad \text{(eq. S7)}$$

The coefficients m and τ determine the curvature of the functional relationship between D, P, and ρ, and D_0 is the initial diffusion coefficient. Thus, the diffusion rate in the cell increased as environmental conditions (habitat suitability and carrying capacity) became less favorable to the species. Also, as abundance approached carrying capacity, the density dependent factor decreased in value and diffusion rate increased. A gradient of diffusion rate between neighboring cells resulted in net movement from less to more suitable habitats or from more crowded to less densely populated areas.

d. Modelling changes in carrying capacity (θ)

Carrying capacity in each cell is assumed to be a function of the unfished biomass ($B_{unfished}$) of the population, the habitat suitability (P_i) and net primary production (NPP_i) in each cell. The global unfished biomass of the population is estimated based on the average of the top-10 annual catches by weight of the modelled species in the world from 1950–2004 and their intrinsic population growth rate. Assuming logistic population growth, unfished biomass ($B_{unfished}$) of a population was estimated:

$B_{unfished} = 4 \cdot MSY/r$ (eq. S8)

We assumed that the average of the top-10 annual catches was roughly equal to the maximum sustainable yield (MSY) of the species. A previous study (*82*) has shown that the top-10 annual catches are strongly and significantly correlated with MSY estimated from survey-based stock assessment. In some cases, the top-10 annual catches may be higher than MSY, with species therefore being over-exploited, or the approach may under-estimate MSY if the species was under-exploited. However, this would not substantially alter the main results from DBEM, which focused largely on the relative changes across time instead of the absolute biomasses or catches. The initial carrying capacity (θ) in each cell is calculated by pro-rating the unfished biomass to each cell based on the predicted habitat suitability. Changes in carrying capacity in each year is proportional to changes predicted habitat suitability and net primary production.

e. Modelling population growth

The model simulated changes in relative abundance of a species by solving the advection-diffusion relationships in eq. (5) first, and then feeding the outputs into a logistic growth function:

$$\frac{dA_i}{dt} = \sum_{j=1}^{N} \quad r \cdot A_i \cdot \left(1 - \frac{A_i}{(\theta_i / \underline{W})}\right) - F \cdot A_i \quad \text{(eq. S9)}$$

where A_i is the abundance in a 30' x 30' cell i, r is the intrinsic population growth, determined through eq. (10). F is the fishing mortality rate, and carrying capacity in biomass is converted to numerical abundance by dividing it with the estimated mean weight . Also:

$$\sum_{t=0}^{t'} \quad e^{-r \cdot a} \cdot l_a \cdot m_a = 1 \qquad \text{(eq. S10)}$$

where t and t' are the age-class and longevity of the population, respectively; l_a is the expected survivorship of females from age 0 to age a, and m_a is the expected number of age-0 female offsprings per individual female or fecundity at age a.

f. Modelling changes in population biomass

In addition to the abundance (A), DBEM calculates a characteristic weight (W) representing the average mass of the population in cell i. The model simulated how changes in temperature and oxygen content (represented by O_2 concentration) would affect growth of the individuals using a sub-model derived from a generalized von Bertalanffy growth function (VBGF).

$$W_t = W_\infty \cdot [1 - e^{-K\cdot(t-t_0)}]^{\frac{1}{1-a}} \qquad \text{(eq. S11)}$$

where W_∞ is the asymptotic weight, and K is the von Bertalanffy growth parameter. For simplification, we assume that the scaling coefficient a = 0.7, with empirical studies showing that a generally varies from 0.50 to 0.95 across fish species, with 2/3 corresponding to the special or standard VBGF.

The model predicts changes in VBGF parameters for each species according to changes in temperature, oxygen and pH in the ocean relative to initial conditions, as:

$$W_\infty = \left(\frac{g\cdot[O_2]\cdot e^{-j_1/T}}{h\cdot[H^+]\cdot e^{-j_2/T}}\right)^{\frac{1}{(1-a)}} \qquad \text{(eq. S12)}$$

$$K = k \cdot (1 - a) \qquad \text{(eq. S13)}$$

in which metabolism is temperature-dependent and aerobic scope is dependent on oxygen availability in the water and maintenance metabolism is affected by physiological stress (e.g., increased acidity). Also, $j = Ea/R$ with Ea and R are the activation energy and Boltzmann constant, respectively, while T is temperature in Kelvin (see Table 1 for default values of j_1 and j_2). In addition, the aerobic scope of marine fishes and invertebrates decreases as temperature approaches

their upper and lower temperature limits (Pörtner 2010). The coefficients *g* and *h* were derived from the average W_∞, *K* and environmental temperature (T_o) of the species reported in literature:

$$g = \frac{{W_\infty}^{1-a} \cdot K}{[O_2] \cdot e^{-j_1/T_0}} \qquad \text{(eq. S14a)}$$

$$h = \frac{K/(1-a)}{[H^+] \cdot e^{-j_2/T_0}} \qquad \text{(eq. S14b)}$$

Adult natural mortality rate (*M*) was estimated from an empirical equation (*51*):

$$M = -0.4851 - 0.0824 \cdot \log(W_{\text{inf}}) + 0.6757 \cdot \log(K) + 0.4687 \cdot \log(T_i) \qquad \text{(eq. S15)}$$

where *T* is the average water temperature in cell *i*.

The estimated growth parameters and natural mortality rate were used in calculating the average body weight of individuals in the population using the length-based life table, where:

$$\underline{W} = \frac{\sum_y \sum_l W_l \cdot X_{l',l} \cdot e^{-M}}{\sum_y \sum_l X_{l',l} \cdot e^{-M}} \qquad \text{(eq. S16)}$$

$X_{l,l'}$ is the probability of an individual growing from length class *l* to *l'* in a time-step (y) as estimated from growth data and W_l is the mean weight of length class *l*.

Thus, average body weight was dependent on temperature and oxygen level. Biomass (*B*) and catch (*C*) were then calculated from the population mean body weight and abundance:

$$B = A \cdot \underline{W} \qquad \text{(eq. S17a)}$$

$$C = A \cdot F \cdot \underline{W} \qquad \text{(eq. S17b)}$$

The model had a spin-up period of 100 years using the climatological average oceanographic conditions from 1971–2000, thereby allowing the population to reach equilibrium before it was

perturbed with oceanographic changes. *F* is exploitation rate. To calculate maximum catch potential and assuming logistic population growth, *F* is set to be equal to natural mortality rate *M* to have maximum equilibrium surplus production.

Illustrative examples

We illustrated the outputs from each step of the integrated models using examples from the west coast of USA and their California sardine (*Engraulis mordax*) stock (Fig. S6 – S8).

Testing the effects of 'marine cold spells'

We examined the projected effects of extreme cold sea surface temperature anomalies that are the inverse of marine annual high temperature extremes (hereafter referred to as 'marine cold spells'). The hypothesis is that marine cold spells are projected to have the same magnitude of effects as marine annual high temperature extremes, but opposite in direction, on potential catches of a stock. To test this hypothesis, we identified the occurrences of marine cold spells in each of the 10 ensemble member projections from the GFDL Earth system model (see above). Marine cold spells were defined as the lower 5-percentile of the sea surface temperature anomalies in an Exclusive Economic Zone (EEZ). Sea surface temperature anomalies were calculated using the same algorithm as for marine annual high temperature extremes. We then calculated the anomalies of the potential catch for each stock in an EEZ when a marine cold snap occurred for all Earth system model ensemble members.

We examined whether the magnitude of the impacts from marine annual high temperature extremes equals to that of marine cold spells on projected catch potential globally and for each EEZ. We analyzed the relationship between catch anomalies from marine annual high temperature extremes and marine cold spells projected from the dynamic bioclimate envelope for

these stocks using a linear mixed effect model (*lmer*) (*lmerTest* package in R), treating each EEZ as a subject (random effect). As it is hypothesized that the effects of cold spells are reciprocal of that of high temperature extremes, we multiple the anomalies of marine cold spells by -1. The model is:

CatchAnom ~lmer[factor(MAE)+(1|EEZ)]

where CatchAnom and MAE are the catch anomalies from marine annual extremes and cold spells while MAE is a factor indicating whether the extremes are high temperature extremes or cold spells, respectively.

Our analysis showed that the impacts from marine cold spells on projected catch potentials are not exactly the inverse of those from marine annual high temperature extremes. The magnitude of impacts of marine cold spells and that from marine annual high temperature extremes are significantly different from one another ($p < 0.05$) (Table S6). Also, there are substantial variabilities between fish stocks, with some stocks being more or less sensitive to marine cold spells relative to marine annual high temperature extremes. Moreover, some stocks were projected to be negatively impacted by both marine annual high temperature extremes and cold spells. Specifically, across all the studied EEZs, the number of stocks that are negatively impacted by annual high temperature extremes (with declines in biomass beyond the rate of decadal-scale mean decrease of 3.6% per decade) are higher than those that are positively impacted by marine cold-spell (biomass increase by more than 3.6%) in 64% of the EEZs. Some of the tropical EEZs have substantially larger number of stocks that are negatively impacted by high temperature extremes than the positive impacts of cold spells e.g., in Ecuador, the Philippines, Ghana.

In summary, when we compare the effects of the inverse of marine annual high temperature extremes ('marine cold spells'), the average impacts after considering both marine annual high temperature extremes and cold spells on projected catch potentials did not cancel each other out. Instead there are substantial variabilities across fish stocks and regions due to their asymmetries in biological sensitivities to ocean warming and cooling at stock and community levels.

Changes in sea bottom temperature during marine annual high temperature extremes in EEZs

We analyzed the relationship between projected sea surface and sea bottom warming during marine annual high temperature extremes. For the years when marine annual high temperature extremes were identified from the 10 ensemble members of the GFDL Earth system model (see Method), we calculated the annual Exclusive Economic Zone (EEZ) averaged sea bottom temperature anomalies relative to the ensemble mean. We tested the relationship between sea surface and sea bottom temperature anomalies, accounting for the variations between EEZ, using a linear mixed effect model (*lmerTest* package in R):

SBTAnom~*lmer*[SSTAnom + (SSTAnom|EEZ)]

Where SBTAnom and SSTAnom are sea bottom and sea surface temperature anomalies, respectively.

Averaged over all EEZs, sea bottom temperature anomalies are significantly and positively correlated with sea surface temperature anomalies (Table S7). However, temperature anomalies at the surface are much bigger than the anomalies near the sea bottom.

Comparison of the range of temperature preferences between pelagic and demersal species

We compared the temperature preference ranges estimated from the dynamic bioclimate envelope model for the pelagic and demersal species included in this study. The dynamic bioclimate envelope model estimated the temperature preference profiles of each species by overlaying each species' distribution and sea water temperature (average of 1971 - 2000, surface for pelagic species and bottom for demersal species). We then calculated the upper and lower temperature ranges above which 5% of the total species distribution were located. The difference between these upper and lower temperature ranges represents the temperature preference range of each species. In the dynamic bioclimate envelope model, the carrying capacity of a habitat is directly proportional to the temperature preference of the species; thus carrying capacity would be low when environmental temperature is close to the species' upper and lower preferred temperature.

We tested the difference in temperature preference ranges between pelagic and demersal species with ANOVA (*lm* function in R). The temperature preference ranges were predicted using the GFDL Earth system model. Since the temperature preference ranges were calculated from 30-year climatological average temperature, interannual variations between different ensemble members of the GFDL Earth system model would not affect the analysis. Thus, this analysis used only one of the 10 ensemble members of the GFDL Earth system model.

Overall, pelagic species have significantly ($p < 0.0001$) narrower temperature preference ranges than demersal species (Table S8).

Evaluating the projections of marine annual high temperature extreme impacts on fisheries with empirical data

We analyzed historical time-series of observation-based sea surface temperature to identify the occurrences of annual marine annual high temperature extremes in each country's Exclusive

Economic Zone(s) (EEZs). We used the Hadley Centre Sea Surface Temperature (SST) gridded data version 1.1 (*83*) and calculated annual average sea surface temperature from 1950 to 2016 for each EEZ. We then applied a decadal running mean filter (9-year average) to the time-series and calculated the annual SST anomalies relative to the filtered SST time-series. A 9-year running mean was applied to remove the decadal temperature trend from the SST time-series. We also tested the sensitivity of the results to alternative windows of running mean (7-year and 11-year). We identified annual marine annual high temperature extremes as the years with SST anomalies that were above the 95th percentile of all the SST anomalies in the time-series (following the same criteria as for identifying marine annual high temperature extremes for the modelled data) (Fig. S10).

Secondly, we analyzed historical time-series of catch data to estimate the changes in annual catch from countries' Exclusive Economic Zones (EEZs) when marine annual high temperature extremes were identified. We used the *Sea Around Us* global catch reconstruction data (www.seaaroundus.org) and extracted the total annual catch estimated to be caught from countries' EEZs for the period 1950-2016. These catch data are herein referred to as "observed data". We only included taxa that were reported at the species level. Similar to the analysis of SST, for each catch time-series, we applied a decadal running mean (9-year average, and tested alternative windows (7-year and 11-year) to remove the long-term decadal trend that may be driven by changes in mean ocean conditions and fishing effort. We then calculated the annual catch anomalies relative to the filtered catch time-series. We assume that the interannual variations in fishing effort over a decade relative to the long-term mean trend largely did not change within the EEZ. We used the entire time-series from 1950-2016 to ensure that we have sufficient samples of marine annual high temperature extremes for each EEZ. According to our definition of marine annual temperature extreme, an average of three high temperature extremes

are identified in each EEZ between 1950 and 2016. The limited sample size increases the challenges to use the observed catch data to statistically evaluate the projected impacts of temperature extremes on catch potential.

We further examined the effects of marine high temperature extremes at each EEZ using the DBEM projected catch potential and SAU catch data. For each EEZ, we tested the effects of high temperature extremes on fisheries as indicated by catch anomalies relative to the decadal-scale mean and used the different studied species as a random effect (allowing for variations in the effects between species). We mapped the effects of marine high temperature extremes based on the DBEM outputs and Sea Around Us catch anomalies, separately, as well as their agreement or disagreement in the direction of impacts. Overall, the effects of marine high temperature events are estimated to be negative in 134 EEZs in based on both DBEM outputs and the Sea Around Us catch anomalies while 20 EEZs are positively impacted (Fig. S11).

Figs. S1 to S11

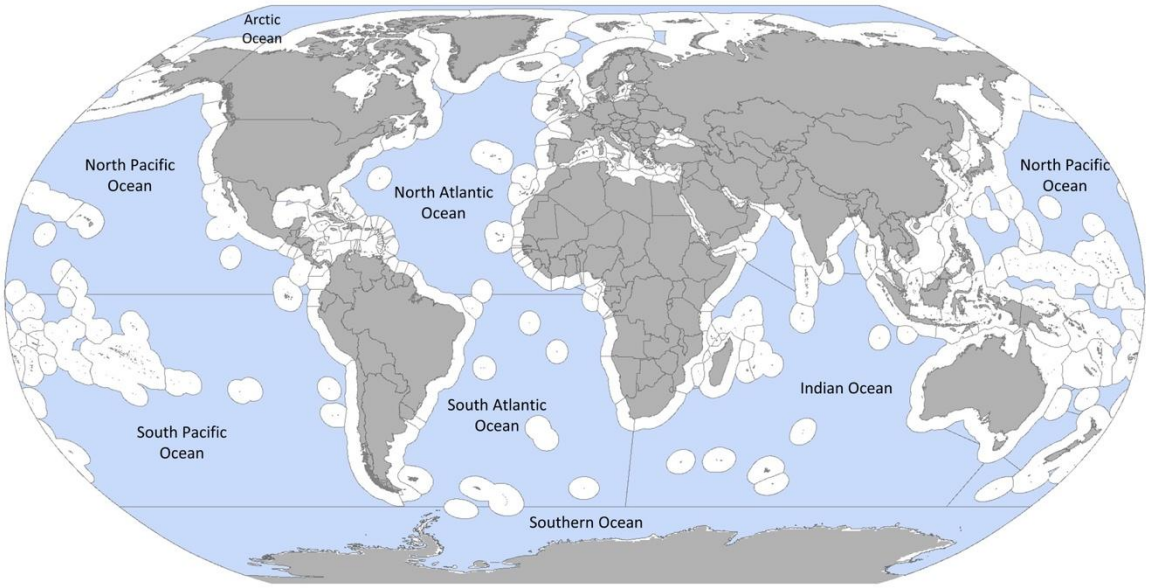

Fig. S1. Exclusive Economic Zones (in white) - regions of the world's ocean.

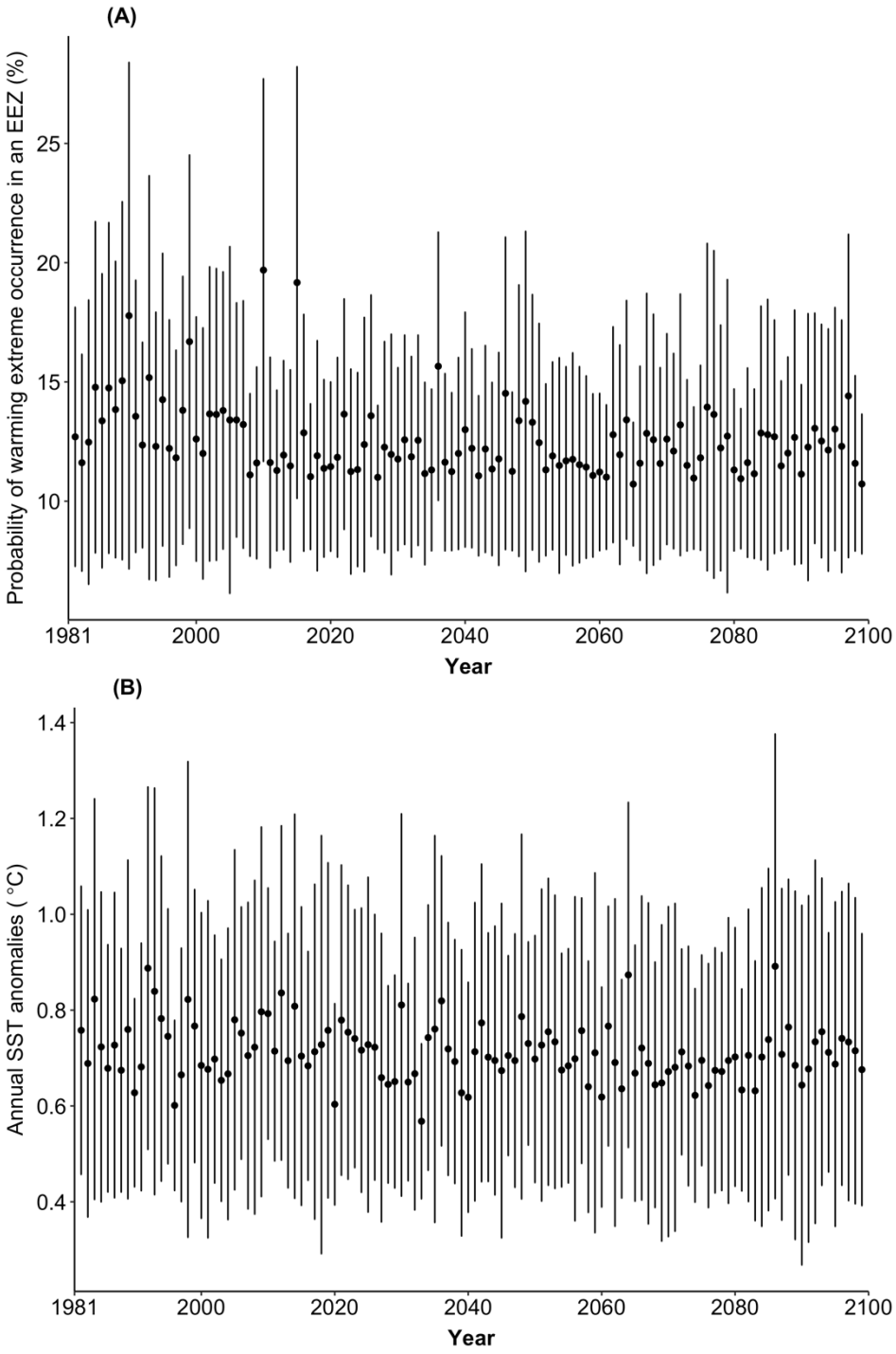

Fig S2. The probability of occurrence and intensity of marine annual high temperature extremes across all Exclusive Economic Zones (EEZs) from 1981 to 2100 under the RCP8.5 scenario. (A) The probability of occurrence of a marine annual high temperature extreme averaged over all EEZs; (B) the intensity of marine annual high temperature extremes averaged over all EEZs indicated by the annual sea surface temperature anomalies of each ensemble

member relative to the ensemble mean. Dark dots represent mean values and the vertical lines represent standard deviation across EEZs. Marine annual high temperature extremes are identified from the projected changes in sea surface temperature (SST) from the 10 ensemble members of GFDL-ESM2M**.** The SST anomalies during a marine annual high temperature extreme decrease very slightly over time (-0.0002^{o}C year^{-1}, $p<0.05$, Table S3) because of the projected reduction in sea surface temperature variability in the tropical Pacific region as reported in previous studies (*83*). Such a trend in temperature variability is characteristic of a subset of Earth system models, including the GFDL-ESM2M employed in this study (*84*). Further studies with additional large ensemble simulations of different Earth system models are needed to examine the robustness of such trend.

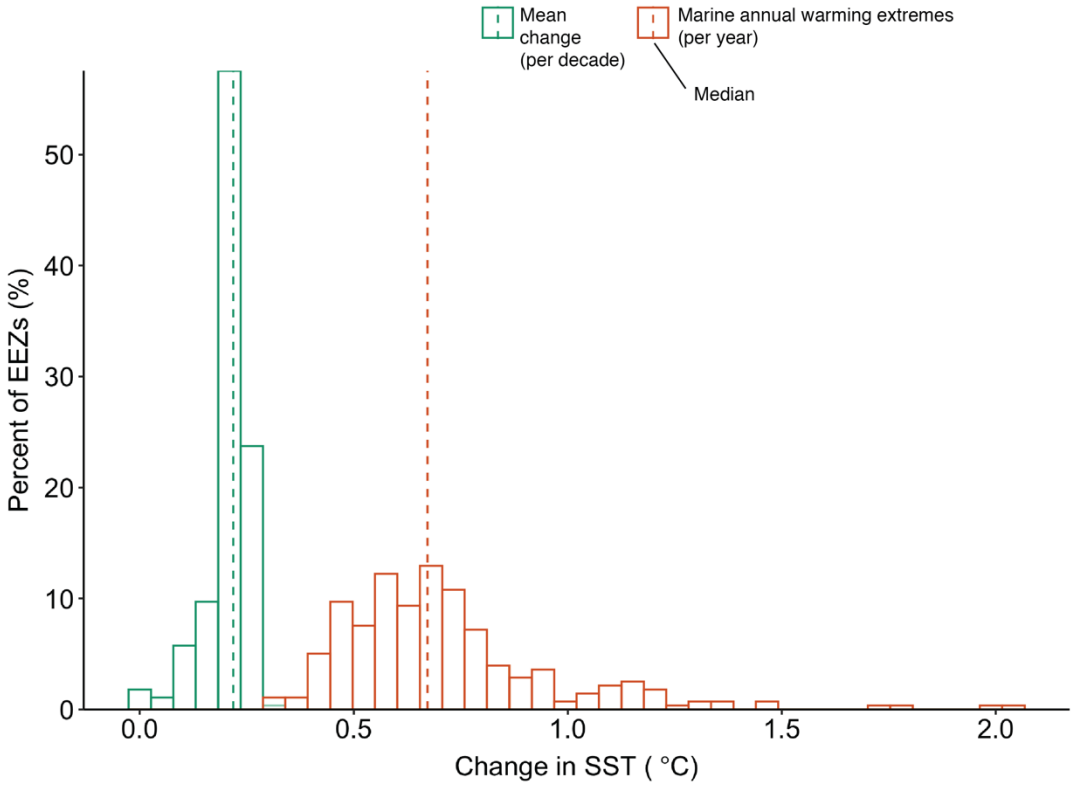

Fig. S3. Distribution of the rate of change in annual mean sea surface temperature (SST) and the average intensity of marine annual high temperature extreme from 1981 to 2100 across all Exclusive Economic Zones (EEZs). The mean rates of SST change across the 10 large ensemble members are estimated by linear regression of annual average SST against time (year). To make the rate of change in temperature comparable between the estimated mean changes and marine annual high temperature extreme, we express the rate of mean change as changes in SST per decade while the rate of marine annual high temperature extreme intensity changes is in SST per year. Assuming a linear change in temperature over this time period in each EEZ, the rate of warming is $0.021 \pm 0.005^{o}C\ year^{-1}$ (Table S3).

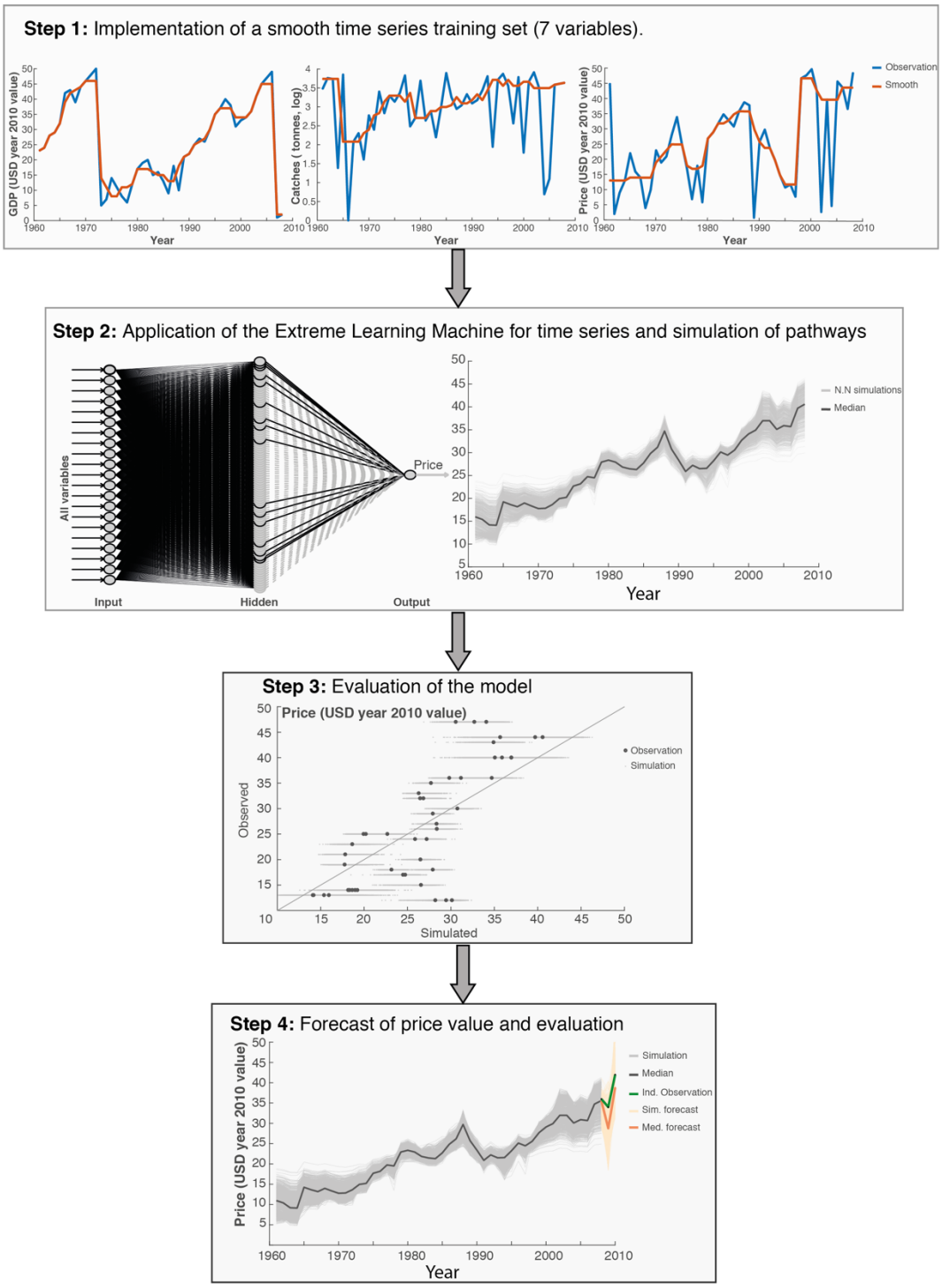

Fig. S4. Illustration of the four main steps in developing and applying an Artificial Neural Network to project ex-vessel prices for the studied fisheries stocks.

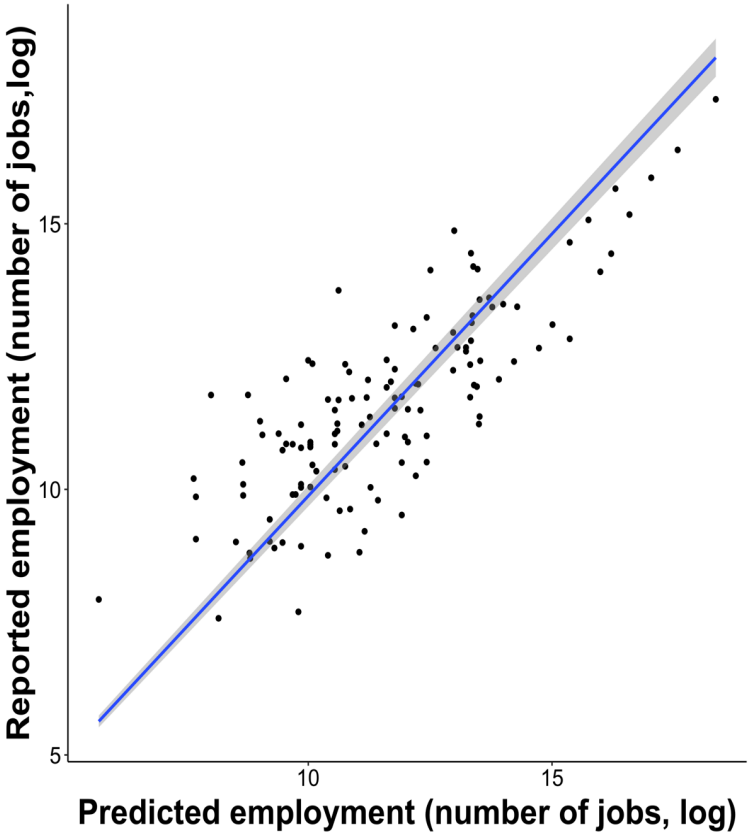

Fig. S5. Reported and predicted total marine employment by countries in the world. The black line represents a linear regression between the observed and predicted employment, which is not significantly different ($p>0.05$, $R^2=0.99$) from a 1:1 relationship.

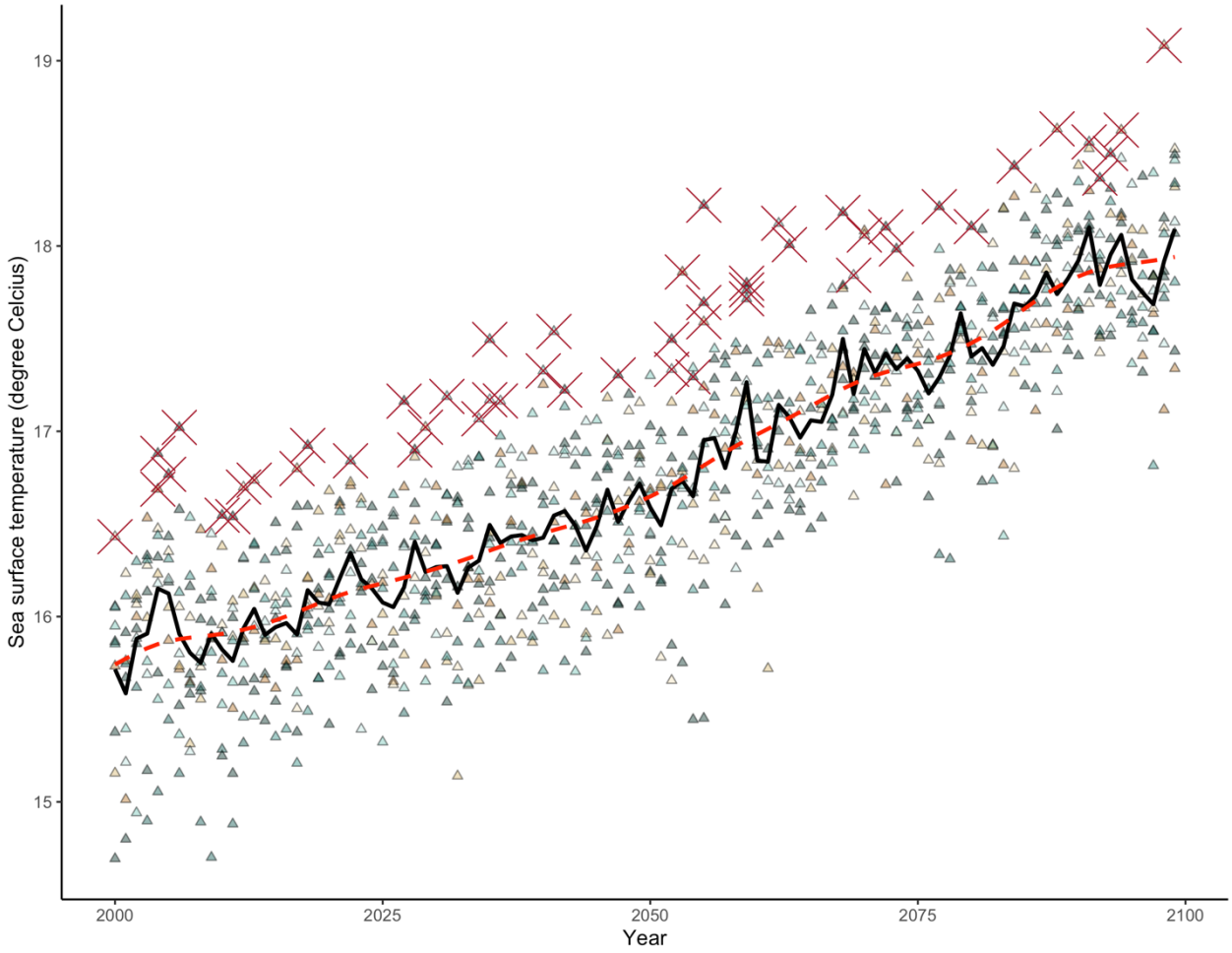

Fig. S6. Projected annual average sea surface temperature in the Exclusive Economic Zone of USA (Pacific Ocean) from 1950 to 2100 from the 10 members of the large ensemble simulations of the GFDL Earth system model (triangles, each colour represents one ensemble member). The red crosses represent the annual average sea surface temperature of identified marine annual high temperature extremes. The black solid line represents the annual average sea surface temperature across ensemble members while the dashed red line represents the smoothed ensemble member-averaged sea surface temperature.

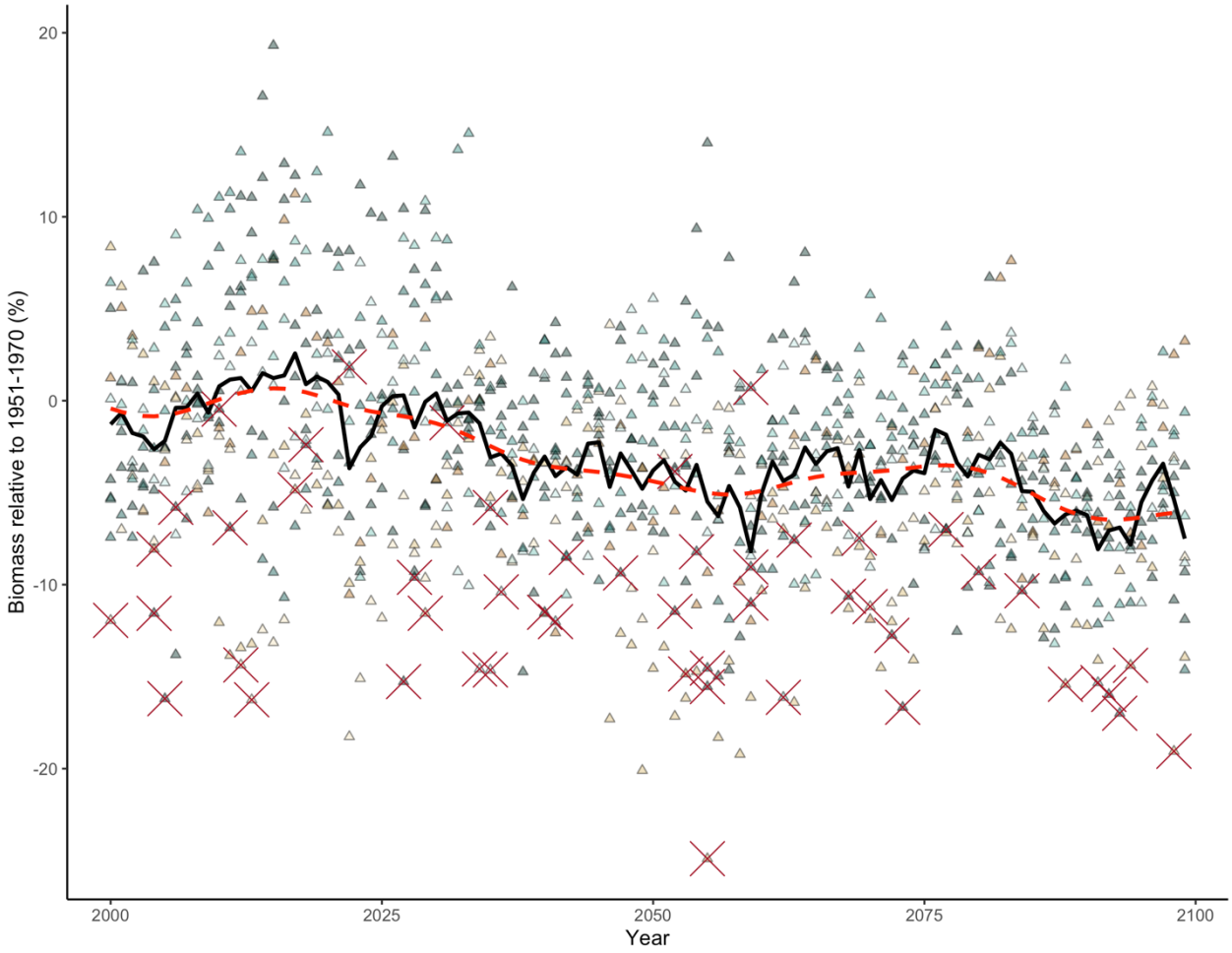

Fig. S7. Changes in projected biomass of California sardine (*Engraulis mordax*) in the Exclusive Economic Zone of USA (Pacific Ocean) relative to the average of 1951 - 1970 as estimated by the DBEM model driven by the 10 members of the large ensemble simulations of the GFDL Earth system model (triangles, each colour represents one ensemble member). The red crosses represent the changes in biomass in years of identified marine annual high temperature extremes. The black solid line represents the annual average changes in biomass across ensemble members while the dashed red line represents the smoothed ensemble member-averaged changes in biomass.

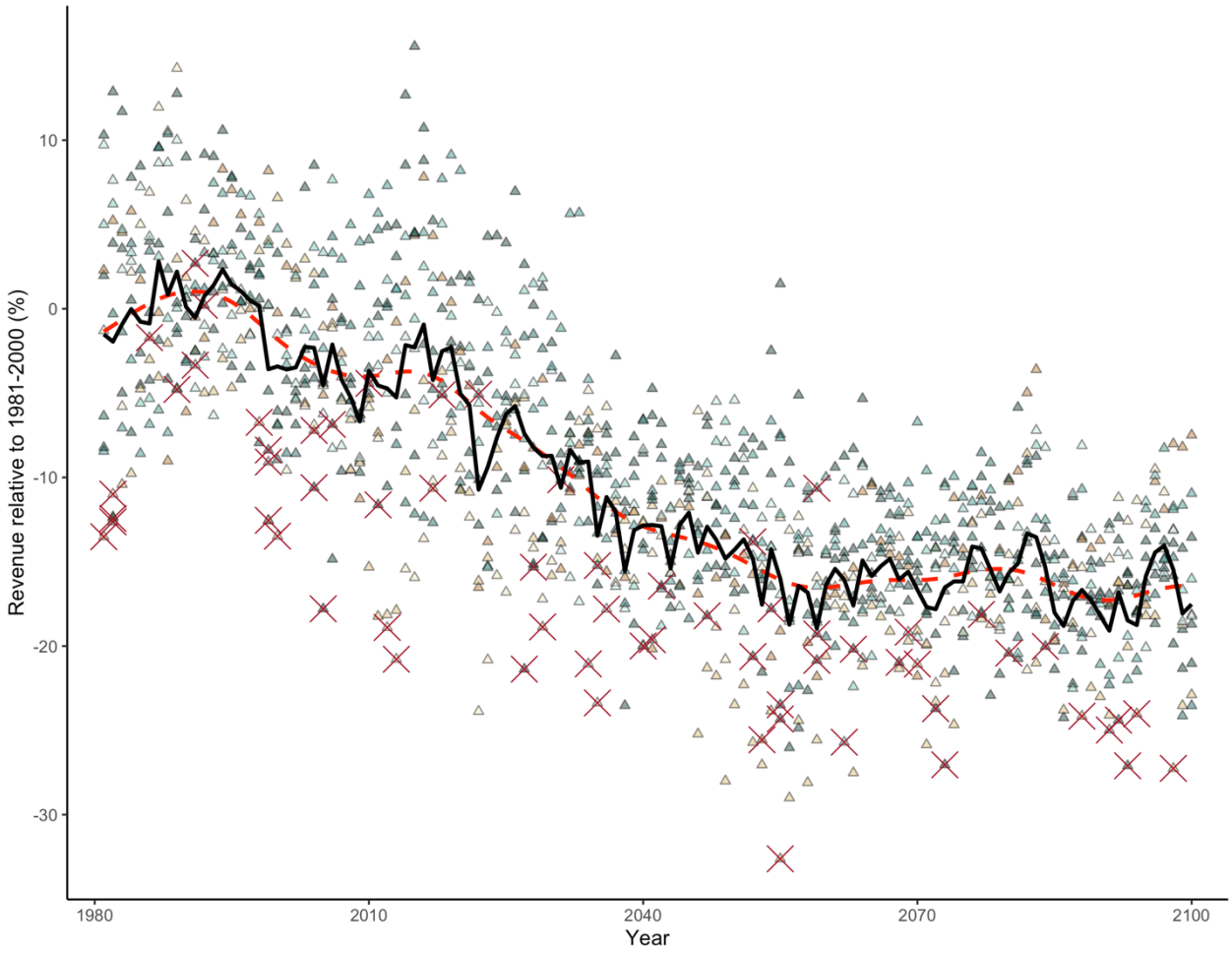

Fig. S8. Changes in projected revenue (project ex-vessel price x catch potential) of California sardine (*Engraulis mordax*) in the Exclusive Economic Zone of USA (Pacific Ocean) relative to the average of 1951 - 1970 by the DBEM model that is driven by the 10 members of the large ensemble simulations of the GFDL Earth system model (triangles, each colour represents one ensemble member). The red crosses represent the changes in revenue in years of identified marine annual high temperature extremes. The black solid line represents the annual average changes in revenue across ensemble members while the dashed red line represents the smoothed ensemble member-averaged changes in revenue.

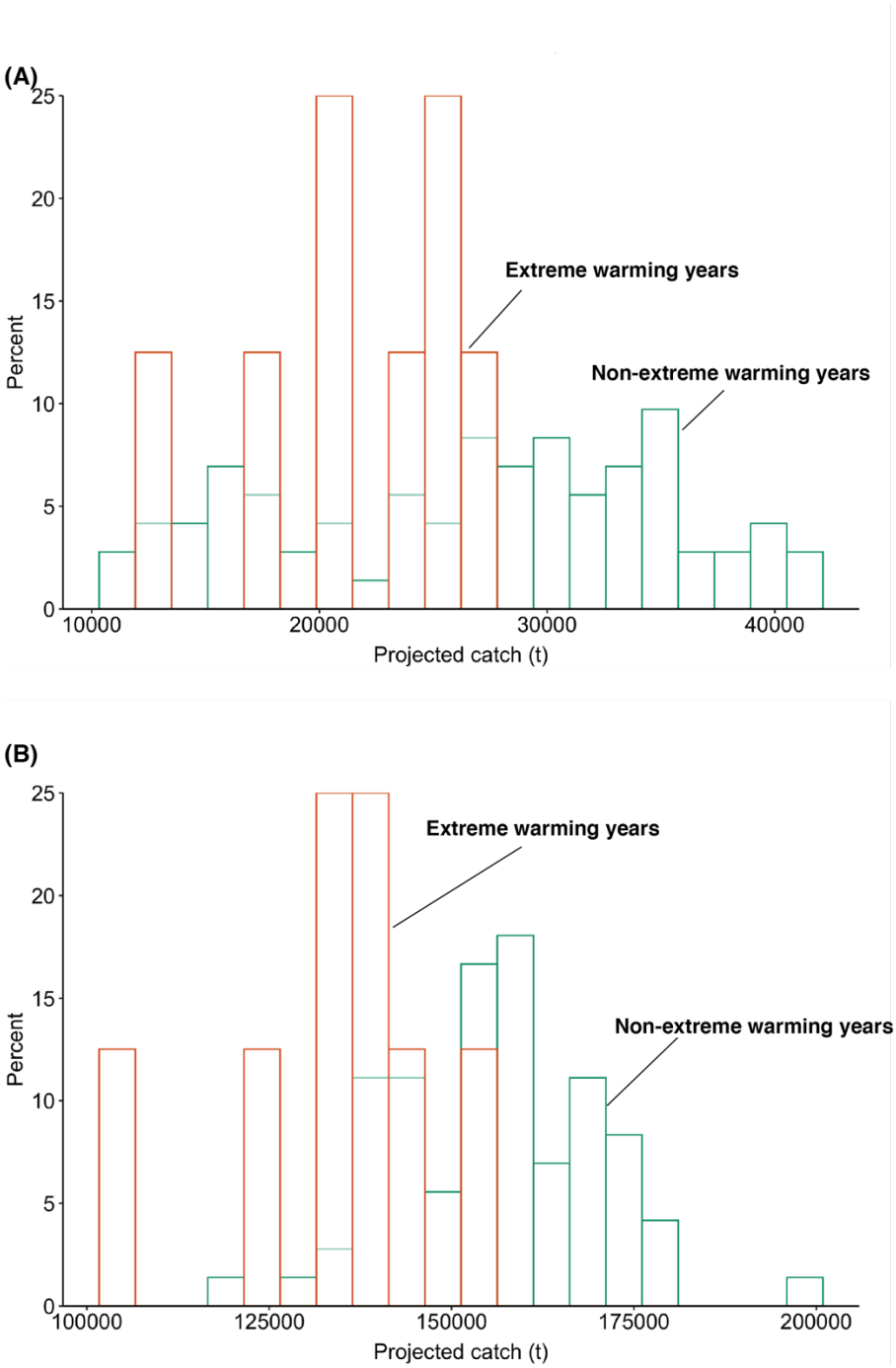

Fig. S9. Distribution of projected total catch from the Exclusive Economic Zone of USA (Pacific Ocean) from 2081 to 2100. (A) Scenarios with harvest control rule fisheries management and (B) no fisheries management.

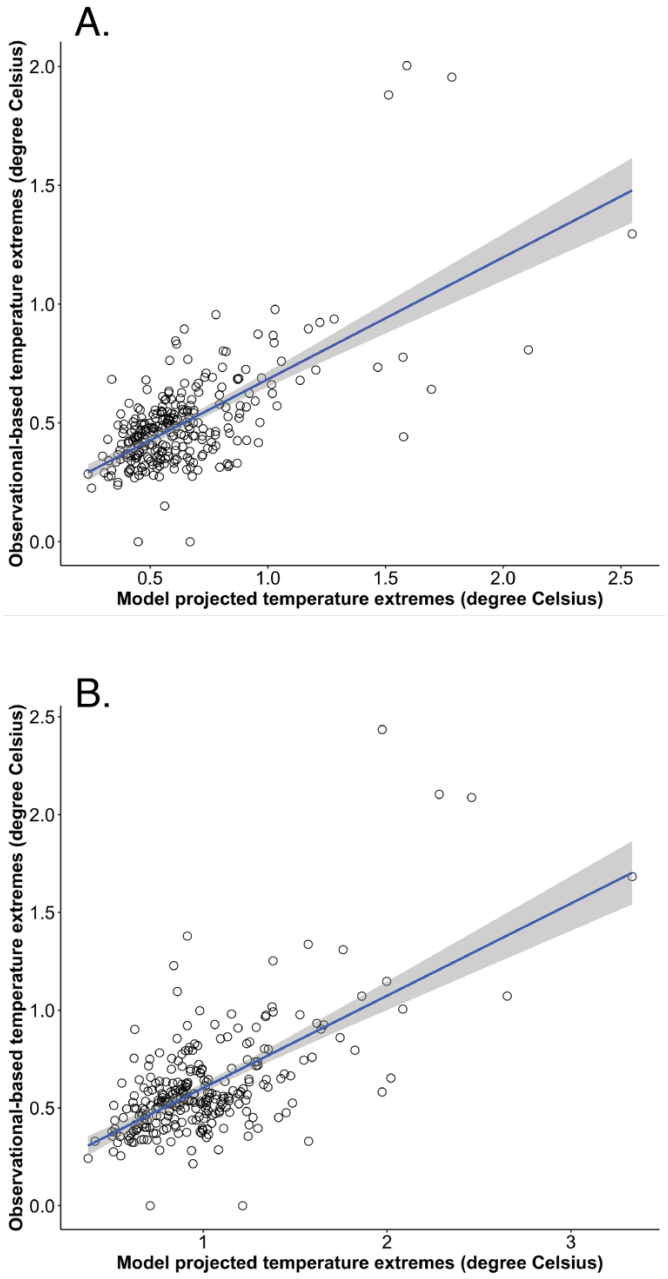

Figure S10. Comparison between annual sea surface temperature anomalies relative to mean conditions by EEZs (A: median, B: maximum) estimated from observed data and model projections during the historical period (1951-2016). The relationships in both (A) and (B), as represented by the regression lines (linear regression) and the 95% confidence intervals (shaded area), are significant at 0.05 level.

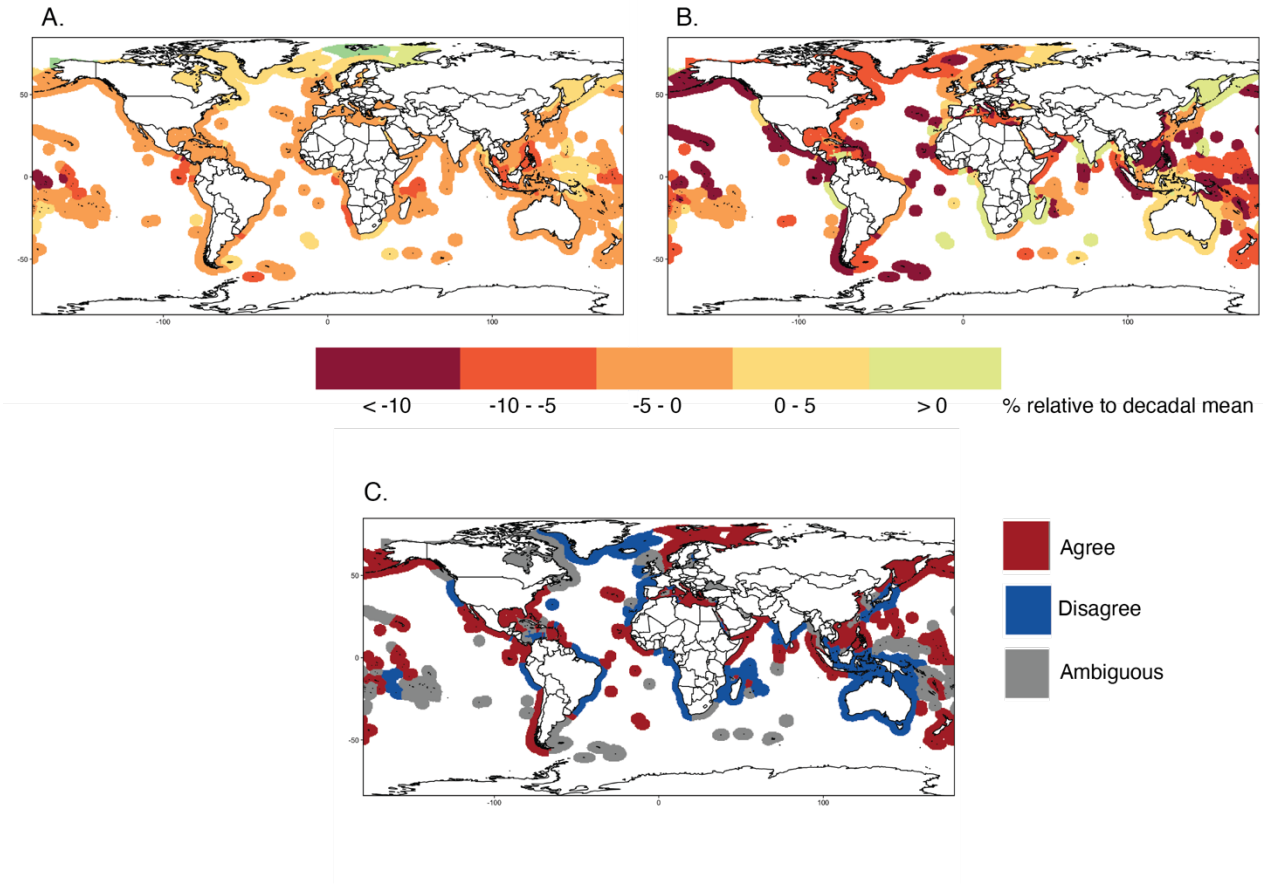

Figure S11. Comparison of estimated average catch anomalies across stocks between *Sea Around Us* catch reconstruction data (www.seaaroundus.org) and the simulated catch potential from the dynamic bioclimate envelope model (DBEM) in the past (1951 – 2016): average catch anomalies from (A) Sea Around Us data and (B) simulated potential catches (% relative to the decadal-scale mean) by EEZ and (C) comparison of the direction of impacts (red: agreement in direction of impacts, blue: disagreement in direction of impacts, grey: ambiguous, meaning that the effects of marine annual temperature extremes estimated from both the model simulations and catch records agree in the direction of changes, but are not significantly different from zero ($p>0.05$).

Table S1 – S8

Table S1. Total catch, proportion of catch from pelagic fishes and the number of fisheries stocks by ocean basin as defined by the United Nations Food and Agriculture Organization (FAO) Statistical Area. For anadromous species, our model represents the marine phase of their life-cycle only.

FAO Area	Total catch [1] (million t)	Proportion from pelagic fishes (%)	Fish stocks[2] (number)	Invertebrate stocks[2] (number)	All stocks[2] (number)
Arctic	0.24	0.06	42	3	45
Northwest Atlantic	2.59	25.36	320	42	362
Northeast Atlantic	8.85	47.46	1844	376	2220
Western Central Atlantic	3.12	33.88	1553	121	1674
Eastern Central Atlantic	3.3	74.83	2328	188	2516
Mediterranean and Black Sea	1.92	72.76	1983	309	2292
Southwest Atlantic	3.67	34.23	377	49	426
Southeast Atlantic	0.96	83.48	442	27	469
Antarctic Atlantic	0.06	0.02	30	3	33
Western Indian Ocean	1.89	73.45	987	59	1046
Eastern Indian Ocean	3.50	74.84	665	95	760
Antarctic, Southern Indian Ocean	0.01	5.24	25	0	25
Northwest Pacific	15.24	23.75	556	126	682
Northeast Pacific	7.39	12.41	170	27	197

Western Central Pacific	7.56	46.39	1266	186	1452
Eastern Central Pacific	1.52	64.21	503	45	548
Southwest Pacific	0.41	9.55	461	22	483
Southeast Pacific	8.61	70.36	243	48	291

1. Total catches from species included in our analysis are based on the Sea Around Us catch database (www.seaaroundus.org) for year 2010.
2. A fish stock is defined by a species occurring in an exclusive economic zone. A stock may occur in two or more FAO area, therefore, the total number stocks across FAO area is more than the total number of assessed stocks in this study.

Table S2. Components of the integrated climate-biodiversity-fisheries-economics impact model and their main outputs, demonstrated performances and main gaps and uncertainties.

Model components	Main outputs*	Demonstrated performance	Main gaps	References
Earth system model GFDL ESM2M	Marine heatwaves and other ocean conditions	The model simulates well the spatial pattern of maximum daily intensity of marine heatwaves with high intensity in the high northern latitudes, the eastern equatorial Pacific and the northern Part of the Southern Ocean. Lower intensities are simulated in the in the subtropical gyres, similar as shown by observations based on the NOAA's daily Optimum Interpolation SST (OISST) analysis product. The GFDL ESM2M model also captures very well the long-term trend in global mean SST over the historical period. Global SST is simulated to increase by 0.13°C decade^{-1} from 1982 to 2019. This is in very close agreement with the observed	The coarse-resolution models of GFDL ESM2M that do not represent well the meso-scale physical and biogeochemical processes that are important in driving large-scale processes of some coastal ecosystems such as eastern boundary upwelling systems.	(*85*, *86*)

		increase of 0.16°C decade^{-1}. Also both the model and the satellite-based observation data indicate an increase of marine heatwave days per year over the 1982-2019 period when defining marine heatwave relative to a fixed 1982-2019 baseline period. In addition, the GFDL ESM2M projections of ocean biogeochemical conditions, such as pH or dissolved oxygen are in close agreement with other CMIP5-type models. In summary, the very good agreement between the simulated present-day heatwave characteristics and the observational-based characteristics, apart from the duration, in addition to the model's fidelity in simulating recent trends in marine heatwave		

		characteristics as well as future ocean biogeochemical conditions gives us great confidence in using this model for analyzing marine heatwave impacts at the global scale.		
Dynamic bioclimate envelope model	Geographic range, biomass and catches	Comparison of projected geographic range of species and occurrence has a median Area Under Curve (AUC) value of 0.82 (target range = 0.5 – 1.0) and projected species number by geographic area is significantly correlated with observations. Projected spatial distribution of maximum catch potential is significantly correlated with reported catches (reported catches are not used in determining the spatial distribution of the catches). Projected changes in total biomass are consistent with projections from six other global marine ecosystem models	Comparison between the model outputs and historical time-series of catch and biomass has not been tested because of the complexity in attributing the observed changes that is due to changes in climate induced changes in catch potential.	(*29*, *87–89*); Supplementary Materials here.

		that are structurally different and tested independently. Projected and observed catches under annual temperature extremes are significantly related.		
Price projection model	Ex-vessel price	Projection for the recent past 10 years significantly related to reported prices.	Ability of the model to project prices with inputs that are substantially out of the same range has not be carried out.	Supplementary Materials here.
Livelihood project model	No. of fisheries-related jobs	Projections from model developed using 75% of reported data significantly related to the values of the remaining 25% of the data reserved for testing	Abilities of the model to project jobs with inputs that are substantially out of the same range and through time have not been tested.	(*90*)
Effort dynamic model (EDM)	Fishing effort and catches	Simulated catches by countries from the EDM are fitted to observed annual catch records from 1950 to 2014. Simulated nominal and effective fishing effort agree qualitatively with estimates based on observational data.	Limited observational records on some model parameters such as fishing cost for specific fishing gear type, fishing effort investment/re-investment, stock biomass time-series are available to constraint the model. Also, the model	(*91*)

			framework does not account for non-market data, seasonal non-fishing employment and benefits that change fishing effort. Moreover, non-economic factors affecting individual fisher's decision has not been accounted for. For example, fishers may also make decision based on other factors such as safety issues linked to travel times and weather, traditional preferences, etc.	

* Outputs that are relevant to this study, see Materials and methods,

Table S3. Test statistics of a generalized linear model with poisson distribution between the probability of occurrence of marine annual high temperature extreme in an Exclusive Economic Zone and year from 1981 to 2100.

Factors	Estimate	Standard error	t-value	p-value
Intercept	0.007	0.133	393.94	<0.01
Year	-0.02	<0.001	-20.94	<0.01

Table S4. Test statistics of a linear model between annual average sea surface temperature anomalies during marine annual high temperature extremes in the EEZs and year from 1981 to 2100.

Factors	Estimate	Standard error	t-value	p-value
Intercept	0.7326	0.0065	112.037	<0.01
Year	-0.0002	0.0001	-2.797	<0.01

Table S5. Parameters of the generalized linear models used in predicting fisheries-related employment. Predictions from Model 1 and Model 2 were used and the outputs were averaged and weighted by their Akaike Information Criterion (AIC).

	Estimated (Model 1)	Estimated (Model 2)
Intercept	1.825	4.436
Rural population (*ruralpopulation*, log-transformed)	0.321	3.358
Total catches (*Y*)	0.677	3.354
GDP per capita (25th quartile to median) ($gdppc_2$)	-0.635	-0.986
GDP per capita (median to 75th quartile) ($gdppc_2$)	2.256	-2.026
GDP per capita (75th quartile to maximum) ($gdppc_3$)	2.067	-2.606
GDP per capita (25th quartile to median)*log(Y)	-0.035	NA
GDP per capita (median to 75th quartile)*log(Y)	-0.436	NA
GDP per capita (75th quartile to maximum)*log(Y)	-0.471	NA
AIC	455	464

Table S6. Test statistics of the linear mixed effect model for the relationship between catch anomalies from marine annual high temperature extremes (MAE) and marine cold spells.

Variables	Estimate	Standard error	Degree of freedom	t-value	p-value
Intercept	-1.215	0.233	281	-9.98	<0.0001
Factor(MAE)	-2.312	0.128	19893	-9.52	<0.0001

Table S7. Test statistics of the linear mixed effect model for the relationship between sea surface and sea bottom temperature anomalies during marine annual high temperature extremes.

Variables	Estimate	Standard error	t-value	p-value
Intercept	-0.0064	0.0032	-2.015	0.0439
SSTAnom	0.1508	0.0179	8.417	<0.0001

Table S8. Test statistics of comparison between the temperature preference ranges of pelagic and demersal species.

Coefficients	Estimate	Standard error	t-value	p-value
Intercept	17.46	0.26	66.98	<0.0001
Pelagic	-6.71	0.59	-11.40	<0.0001

REFERENCES AND NOTES

1. U. R. Sumaila, W. Cheung, A. Dyck, K. Gueye, L. Huang, V. Lam, D. Pauly, T. Srinivasan, W. Swartz, R. Watson, D. Zeller, Benefits of rebuilding global marine fisheries outweigh costs. *PLOS ONE* **7**, e40542 (2012).
2. FAO, *The State of World Fisheries and Aquaculture 2018–Meeting the Sustainable Development Goals* (FAO, 2018).
3. C. C. Hicks, P. J. Cohen, N. A. J. Graham, K. L. Nash, E. H. Allison, C. D'Lima, D. J. Mills, M. Roscher, S. H. Thilsted, A. L. Thorne-Lyman, M. Aaron MacNeil, Harnessing global fisheries to tackle micronutrient deficiencies. *Nature* **574**, 95–98 (2019).
4. L. C. L. Teh, U. R. Sumaila, Contribution of marine fisheries to worldwide employment. *Fish Fish.* **14**, 77–88 (2013).
5. A. M. Cisneros-Montemayor, D. Pauly, L. V. Weatherdon, Y. Ota, A global estimate of seafood consumption by coastal indigenous peoples. *PLOS ONE* **11**, e0166681 (2016).
6. IPCC, *Summary for Policymakers. In: IPCC Special Report on the Ocean and Cryosphere in a Changing Climate* (IPCC, 2019).
7. K. M. A. Chan, J. Agard, J. Liu, A. P. D. de Aguiar, D. Armenteras-Pascual, A. K. Boedhihartono, William. W. L. Cheung, S. Hashimoto, G. C. H. Pedraza, T. Hickler, J. Jetzkowitz, M. Kok, M. Murray-Hudson, P. O'Farrell, T. Satterfield, A. K. Saysel, R. Seppelt, B. Strassburg, D. Xue, *IPBES Global Assessment on Biodiversity and Ecosystem Services* (Intergovernmental Science-Policy Platform on Biodiversity and Ecosystem Services, 2019).
8. H. K. Lotze, D. P. Tittensor, A. Bryndum-Buchholz, T. D. Eddy, W. W. L. Cheung, E. D. Galbraith, M. Barange, N. Barrier, D. Bianchi, J. L. Blanchard, L. Bopp, M. Büchner, C. M. Bulman, D. A. Carozza, V. Christensen, M. Coll, J. P. Dunne, E. A. Fulton, S. Jennings, M. C. Jones, S. Mackinson, O. Maury, S. Niiranen, R. Oliveros-Ramos, T. Roy, J. A. Fernandes, Jacob Schewe, Y.-J. Shin, T. A. M. Silva, J. Steenbeek, C. A. Stock, P. Verley, J. Volkholz, N. D. Walker, B. Worm, Global ensemble projections reveal trophic amplification of ocean biomass declines with climate change. *Proc. Natl. Acad. Sci.* **116**, 12907–12912 (2019).
9. W. W. L. Cheung, G. Reygondeau, T. L. Frölicher, Large benefits to marine fisheries of meeting the 1.5 C global warming target. *Science* **354**, 1591–1594 (2016).
10. V. W. Y. Lam, W. W. L. Cheung, G. Reygondeau, U. R. Sumaila, Projected change in global fisheries revenues under climate change. *Sci. Rep.* **6**, 32607 (2016).

11. U. R. Sumaila, T. C. Tai, V. W. Y. Lam, W. W. L. Cheung, M. Bailey, A. M. Cisneros-Montemayor, O. L. Chen, S. S. Gulati, Benefits of the Paris Agreement to ocean life, economies, and people. *Sci. Adv.* **5**, eaau3855 (2019).
12. C. Laufkötter, T. L. Frölicher, J. Zscheischler, High-impact marine heatwaves attributable to human-induced global warming. *Science* **369**, 1621–1625 (2020).
13. T. L. Frölicher, E. M. Fischer, N. Gruber, Marine heatwaves under global warming. *Nature* **560**, 360–364 (2018).
14. A. J. Hobday, L. V Alexander, S. E. Perkins, D. A. Smale, S. C. Straub, E. C. J. Oliver, J. A. Benthuysen, M. T. Burrows, M. G. Donat, M. Feng, N. J. Holbrook, P. J. Moore, H. A. Scannell, A. S. Gupta, T. Wernberg, A hierarchical approach to defining marine heatwaves. *Prog. Oceanogr.* **141**, 227–238 (2016).
15. T. L. Frölicher, C. Laufkötter, Emerging risks from marine heat waves. *Nat. Commun.* **9**, 650 (2018).
16. L. M. Cavole, A. M. Demko, R. E. Diner, A. Giddings, I. Koester, C. M. L. S. Pagniello, M. L. Paulsen, A. Ramirez-Valdez, S. M. Schwenck, N. K. Yen, M. E. Zill, P. J. S. Franks, Biological impacts of the 2013–2015 warm-water anomaly in the northeast Pacific: Winners, losers, and the future. *Oceanography* **29**, 273–285 (2016).
17. J. A. Benthuysen, E. C. J. Oliver, K. Chen, T. Wernberg, Editorial: Advances in understanding marine heatwaves and their impacts. *Front. Mar. Sci.* **7**, 147 (2020).
18. J. F. Piatt, J. K. Parrish, H. M. Renner, S. K. Schoen, T. T. Jones, M. L. Arimitsu, K. J. Kuletz, B. Bodenstein, M. García-Reyes, R. S. Duerr, R. M. Corcoran, R. S. A. Kaler, G. J. McChesney, R. T. Golightly, H. A. Coletti, R. M. Suryan, H. K. Burgess, J. Lindsey, K. Lindquist, P. M. Warzybok, J. Jahncke, J. Roletto, W. J. Sydeman, Extreme mortality and reproductive failure of common murres resulting from the northeast Pacific marine heatwave of 2014-2016. *PLOS ONE* **15**, e0226087 (2020).
19. T. P. Hughes, J. T. Kerry, M. Álvarez-Noriega, J. G. Álvarez-Romero, K. D. Anderson, A. H. Baird, R. C. Babcock, M. Beger, D. R. Bellwood, R. Berkelmans, T. C. Bridge, I. R. Butler, M. Byrne, N. E. Cantin, S. Comeau, S. R. Connolly, G. S. Cumming, S. J. Dalton, G. Diaz-Pulido, C. M. Eakin, W. F. Figueira, J. P. Gilmour, H. B. Harrison, S. F. Heron, A. S. Hoey, J.-P. A. Hobbs, M. O. Hoogenboom, E. V. Kennedy, C.-y. Kuo, J. M. Lough, R. J. Lowe, G. Liu, M. T. McCulloch, H. A. Malcolm, M. J.. McWilliam, J. M. Pandolfi, R. J. Pears, M. S. Pratchett, V. Schoepf, T. Simpson, W.

J. Skirving, B. Sommer, G. Torda, D. R. Wachenfeld, B. L. Willis, S. K. Wilson, Global warming and recurrent mass bleaching of corals. *Nature* **543**, 373–377 (2017).

20. T. Wernberg, D. A. Smale, F. Tuya, M. S. Thomsen, T. J. Langlois, T. De Bettignies, S. Bennett, C. S. Rousseaux, An extreme climatic event alters marine ecosystem structure in a global biodiversity hotspot. *Nat. Clim. Chang.* **3**, 78–82 (2013).
21. N. L. Bindoff, W. W. L. Cheung, J. G. Kairo, J. Arístegui, V. A. Guinder, R. Hallberg, N. Hilmi, N. Jiao, M. saiful Karim, L. Levin, S. O'Donoghue, S. R. Purca Cuicapusa, B. Rinkevich, T. Suga, A. Tagliabue, P. Williamson, "Changing ocean, marine ecosystems, and dependent communities, in *Special Report on the Ocean and Cryosphere in a Changing Climate* (IPCC, 2019).
22. D. A. Smale, T. Wernberg, E. C. J. Oliver, M. Thomsen, B. P. Harvey, S. C. Straub, M. T. Burrows, L. V. Alexander, J. A. Benthuysen, M. G. Donat, M. Feng, A. J. Hobday, N. J. Holbrook, S. E. Perkins-Kirkpatrick, H. A. Scannell, A. S. Gupta, B. L. Payne, P. J. Moore, Marine heatwaves threaten global biodiversity and the provision of ecosystem services. *Nat. Clim. Chang.* **9**, 306–312 (2019).
23. N. M. Wade, T. D. Clark, B. T. Maynard, S. Atherton, R. J. Wilkinson, R. P. Smullen, R. S. Taylor, Effects of an unprecedented summer heatwave on the growth performance, flesh colour and plasma biochemistry of marine cage-farmed Atlantic salmon (Salmo salar). *J. Therm. Biol.* **80**, 64–74 (2019).
24. W. W. L. Cheung, T. L. Frölicher, Marine heatwaves exacerbate climate change impacts for fisheries in the northeast Pacific. *Sci. Rep.* **10**, 6678 (2020).
25. F. A. Burger, T. L. Frölicher, J. G. John, Increase in ocean acidity variability and extremes under increasing atmospheric CO_2. *Biogeosciences* **17**, 4633–4662 (2020).
26. E. C. J. Oliver, J. A. Benthuysen, S. Darmaraki, M. G. Donat, A. J. Hobday, N. J. Holbrook, R. W. Schlegel, A. Sen Gupta, Marine heatwaves. *Annu. Rev. Mar. Sci.* **13**, 313–342 (2021).
27. W. W. L. Cheung, M. A. Oyinlola, Dynamic integrated marine climate, biodiversity, fisheries, aquaculture and seafood market model (DIVERSE), in *Fisheries Centre Research Report* (Institute for the Oceans and Fisheries, The University of British Columbia, 2019), vol. 27.
28. D. Pauly, D. Zeller, M. D. Palomares, *Sea Around Us Concepts, Design and Data* (2020); www.seaaroundus.org.

29. W. W. L. Cheung, M. C. Jones, G. Reygondeau, C. A. Stock, V. W. Y. Lam, T. L. Frölicher, Structural uncertainty in projecting global fisheries catches under climate change. *Ecol. Model.* **325**, 57–66 (2016).
30. J. Marshall, K. Speer, Closure of the meridional overturning circulation through Southern Ocean upwelling. *Nat. Geosci.* **5**, 171–180 (2012).
31. E. C. J. Oliver, M. G. Donat, M. T. Burrows, P. J. Moore, D. A. Smale, L. V. Alexander, J. A. Benthuysen, M. Feng, A. S. Gupta, A. J. Hobday, N. J. Holbrook, S. E. Perkins-Kirkpatrick, H. A. Scannell, S. C. Straub, T. Wernberg, tLonger and more frequent marine heatwaves over the past century. *Nat. Commun.* **9**, 1324 (2018).
32. N. Le Grix, J. Zscheischler, C. Laufkötter, C. S. Rousseaux, T. L. Frölicher, Compound high-temperature and low-chlorophyll extremes in the ocean over the satellite period. *Biogeosciences* **18**, 2119–2137 (2021).
33. M. B. Araújo, F. Ferri-Yáñez, F. Bozinovic, P. A. Marquet, F. Valladares, S. L. Chown, Heat freezes niche evolution. *Ecol. Lett.* **16**, 1206–1219 (2013).
34. M. D. Robertson, J. Gao, P. M. Regular, M. J. Morgan, F. Zhang, Lagged recovery of fish spatial distributions following a cold-water perturbation. *Sci. Rep.* **11**, 9513 (2021).
35. J. M. Sunday, A. E. Bates, N. K. Dulvy, Thermal tolerance and the global redistribution of animals. *Nat. Clim. Chang.* **2**, 686–690 (2012).
36. M. Lima, D. E. Naya, Large-scale climatic variability affects the dynamics of tropical skipjack tuna in the Western Pacific Ocean. *Ecography* **34**, 597–605 (2011).
37. W. Cornwall, Ocean heat waves like the Pacific's deadly "Blob" could become the new normal. *Science* (2019).
38. K. E. Mills, A. J. Pershing, C. J. Brown, Y. Chen, F.-S. Chiang, D. S. Holland, S. Lehuta, J. A. Nye, J. C. Sun, A. C. Thomas, R. A. Wahle, Fisheries management in a changing climate: Lessons from the 2012 ocean heat wave in the Northwest Atlantic. *Oceanography* **26**, 191–195 (2013).
39. E. C. J. Oliver, J. A. Benthuysen, N. L. Bindoff, A. J. Hobday, N. J. Holbrook, C. N. Mundy, S. E. Perkins-Kirkpatrick, The unprecedented 2015/16 Tasman Sea marine heatwave. *Nat. Commun.* **8**, 16101 (2017).
40. V. W. Y. Lam, A. Cineros-Montemayor, W. W. L. Cheung, in *Dynamic Integrated Marine Climate, Biodivesity, Fisheries, Aquaculture and Seafood Market Model (DIVERSE)*, W. W. L. Cheung, M. A. Oyinlola, Eds. (Institute for the Oceans and Fisheries, The University of British Columbia, 2019).

41. S. D. Gaines, C. Costello, B. Owashi, T. Mangin, J. Bone, J. G. Molinos, M. Burden, H. Dennis, B. S. Halpern, C. V. Kappel, K. M. Kleisner, D. Ovando, Improved fisheries management could offset many negative effects of climate change. *Sci. Adv.* **4**, eaao1378 (2018).
42. C. M. Free, T. Mangin, J. G. Molinos, E. Ojea, M. Burden, C. Costello, S. D. Gaines, Realistic fisheries management reforms could mitigate the impacts of climate change in most countries. *PLOS ONE* **15**, e0224347 (2020).
43. R. M. Suryan, M. L. Arimitsu, H. A. Coletti, R. R. Hopcroft, M. R. Lindeberg, S. J. Barbeaux, S. D. Batten, W. J. Burt, M. A. Bishop, J. L. Bodkin, R. Brenner, R. W. Campbell, D. A. Cushing, S. L. Danielson, M. W. Dorn, B. Drummond, D. Esler, T. Gelatt, D. H. Hanselman, S. A. Hatch, S. Haught, K. Holderied, K. Iken, D. B. Irons, A. B. Kettle, D. G. Kimmel, B. Konar, K. J. Kuletz, B. J. Laurel, J. M. Maniscalco, C. Matkin, C. A. E. McKinstry, D. H. Monson, J. R. Moran, D. Olsen, W. A. Palsson, W. S. Pegau, J. F. Piatt, L. A. Rogers, N. A. Rojek, A. Schaefer, I. B. Spies, J. M. Straley, S. L. Strom, K. L. Sweeney, M. Szymkowiak, B. P. Weitzman, E. M. Yasumiishi, S. G. Zador, Ecosystem response persists after a prolonged marine heatwave. *Sci. Rep.* **11**, 6235 (2021).
44. C. A. Stock, M. A. Alexander, N. A. Bond, K. M. Brander, W. W. L. Cheung, E. N. Curchitser, T. L. Delworth, J. P. Dunne, S. M. Griffies, M. A. Haltuch, J. A. Hare, A. B. Hollowed, P. Lehodey, S. A. Levin, J. S. Link, K. A. Rose, R. R. Rykaczewski, J. L. Sarmiento, R. J. Stouffer, F. B. Schwing, G. A. Vecchi, F. E. Werner, On the use of IPCC-class models to assess the impact of climate on Living Marine Resources. *Prog. Oceanogr.* **88**, 1–27 (2011).
45. L. Suarez-Gutierrez, S. Milinski, N. Maher, Exploiting large ensembles for a better yet simpler climate model evaluation. *Clim. Dyn.* (2021).
46. E. D. Houde, in *Fish Reproductive Biology* (John Wiley & Sons, 2016), pp. 98–187.
47. L. Bopp, L. Resplandy, J. C. Orr, S. C. Doney, J. P. Dunne, M. Gehlen, P. Halloran, C. Heinze, T. Ilyina, R. Séférian, J. Tjiputra, M. Vichi, Multiple stressors of ocean ecosystems in the 21st century: Projections with CMIP5 models. *Biogeosciences* **10**, 6225–6245 (2013).
48. D. Pauly, D. Zeller, Catch reconstructions reveal that global marine fisheries catches are higher than reported and declining. *Nat. Commun.* **7**, 10244 (2016).
49. L. W. Botsford, J. C. Castilla, C. H. Peterson, The management of fisheries and marine ecosystems. *Science* **277**, 509–515 (1997).
50. S. M. Griffies, Elements of the modular ocean model (MOM). *GFDL Ocean Group Tech. Rep.* **7**, 47 (2012).

51. T. L. Frölicher, K. B. Rodgers, C. A. Stock, W. W. L. Cheung, Sources of uncertainties in 21st century projections of potential ocean ecosystem stressors. *Glob. Biogeochem. Cycles* **30**, 1224–1243 (2016).
52. K. E. Taylor, R. J. Stouffer, G. A. Meehl, An overview of CMIP5 and the experiment design. *Bull. Am. Meteorol. Soc.* **93**, 485–498 (2012).
53. K. B. Rodgers, J. Lin, T. L. Frölicher, Emergence of multiple ocean ecosystem drivers in a large ensemble suite with an earth system model. *Biogeosciences* **11**, 18189–18227 (2015).
54. T. L. Frölicher, L. Ramseyer, C. C. Raible, K. B. Rodgers, J. Dunne, Potential predictability of marine ecosystem drivers. *Biogeosciences* **17**, 2061–2083 (2020).
55. M. G. Jacox, M. A. Alexander, S. J. Bograd, J. D. Scott, Thermal displacement by marine heatwaves. *Nature* **584**, 82–86 (2020).
56. E. C. J. Oliver, Mean warming not variability drives marine heatwave trends. *Clim. Dyn.* **53**, 1653–1659 (2019).
57. William. W. L. Cheung, V. W. Y. Lam, D. Pauly, in *Modelling Present and Climate-shifted Distributions of Marine Fishes and Invertebrates*, William. W. L. Cheung, V. W. Y. Lam, D. Pauly, Eds. (The University of British Columbia, 2008), vol. 16, pp. 5–50.
58. W. W. L. Cheung, R. Watson, D. Pauly, Signature of ocean warming in global fisheries catch. *Nature* **497**, 365–368 (2013).
59. D. Pauly, On the interrelationships between natural mortality, growth parameters, and mean environmental temperature in 175 fish stocks. *J. Cons. Int. Explor. Mer* **39**, 175–192. (1980).
60. T. C. Tai, T. Cashion, V. W. Y. Lam, W. Swartz, U. R. Sumaila, Ex-vessel fish price database: Disaggregating prices for low-priced species from reduction fisheries. *Front. Mar. Sci.* **4**, 363 (2017).
61. N. Kourentzes, D. K. Barrow, S. F. Crone, Neural network ensemble operators for time series forecasting. *Expert Syst. Appl.* **41**, 4235–4244 (2014).
62. L. Nguyen, H. W. Kinnucan, Effects of income and population growth on fish price and welfare. *Aquac. Econ. Manag.* **22**, 244–263 (2018).
63. J. Guillen, F. Maynou, Characterisation of fish species based on ex-vessel prices and its management implications: An application to the Spanish Mediterranean. *Fish. Res.* **167**, 22–29 (2015).

64. C. Costello, D. Ovando, T. Clavelle, C. Kent Strauss, R. Hilborn, M. C. Melnychuk, T. A. Branch, S. D. Gaines, C. S. Szuwalski, R. B. Cabral, D. N. Rader, A. Leland, Global fishery prospects under contrasting management regimes. *Proc. Natl. Acad. Sci.* **113**, 5125–5129 (2016).
65. R. Summers, International price comparisons based upon incomplete DATA*. *Rev. Income Wealth* **19**, 1–16 (1973).
66. W. Swartz, R. Sumaila, R. Watson, Global ex-vessel fish price database revisited: A new approach for estimating 'Missing' Prices. *Environ. Resour. Econ.* **56**, 467–480 (2013).
67. A. Heston, R. Summers, B. Aten, Penn World Table Version 7.1, Center for International Comparisons of Production, Income and Prices at the University of Pennsylvania, Philadelphia (CHASS Data Centre, 2012).
68. C. C. C. Wabnitz, L. Teh, W. W. L. Cheung, in *Dynamic Integrated Marine Climate, Biodiveristy, Fisheries, Aquaculture and Seafood Market Model (DIVERSE)*, W. W. L. Cheung, M. A. Oyinlola, Eds. (Institute for the Oceans and Fisheries, The University of British Columbia, 2019).
69. M. B. Schaefer, Some considerations of population dynamics and economics in relation to the management of the commercial marine fisheries. *J. Fish. Board Can.* **14**, 669–681 (1957).
70. V. W. Y. Lam, U. R. Sumaila, A. Dyck, D. Pauly, R. Watson, Construction and first applications of a global cost of fishing database. *ICES J. Mar. Sci.* **68**, 1996–2004 (2011).
71. U. R. Sumaila, D. Pauly, "Catching more bait: A bottom-up re-estimation of global fisheries subsidies" (Fisheries Centre, University of British Columbia, 2006).
72. U. R. Sumaila, V. Lam, F. Le Manach, W. Swartz, D. Pauly, Global fisheries subsidies: An updated estimate. *Mar. Policy* **69**, 189–193 (2016).
73. B. C. O'Neill, E. Kriegler, K. Riahi, K. L. Ebi, S. Hallegatte, T. R. Carter, R. Mathur, D. P. van Vuuren, A new scenario framework for climate change research: The concept of shared socioeconomic pathways. *Clim. Chang.* **122**, 387–400 (2014).
74. K. Riahi, D. P. van Vuuren, E. Kriegler, J. Edmonds, B. C. O'Neill, S. Fujimori, N. Bauer, K. Calvin, R. Dellink, O. Fricko, W. Lutz, A. Popp, J. C. Cuaresma, S. KC, M. Leimbach, L. Jiang, T. Kram, S. Rao, J. Emmerling, K. Ebi, T. Hasegawa, P. Havlik, F. Humpenöder, L. A. Da Silva, S. Smith, E. Stehfest, V. Bosetti, J. Eom, D. Gernaat, T. Masui, J. Rogelj, J. Strefler, L. Drouet, V. Krey, G. Luderer, M. Harmsen, K. Takahashi, L. Baumstark, J. C. Doelman, M. Kainuma, Z. Klimont, G. Marangoni, H. Lotze-Campen, M. Obersteiner, A. Tabeau, M. Tavoni, The shared

socioeconomic pathways and their energy, land use, and greenhouse gas emissions implications: An overview. *Glob. Environ. Chang.* **42**, 153–168 (2017).

75. B. Jones, B. C. O'Neill, Spatially explicit global population scenarios consistent with the Shared Socioeconomic Pathways. *Environ. Res. Lett.* **11**, 84003 (2016).
76. D. Zeller, M. L. D. Palomares, A. Tavakolie, M. Ang, D. Belhabib, W. W. L. Cheung, V. W. Y. Lam, E. Sy, G. Tsui, K. Zylich, D. Pauly, Still catching attention: Sea Around Us reconstructed global catch data, their spatial expression and public accessibility. *Mar. Policy* **70**, 145–152 (2016).
77. W. G. Harrison, G. F. Cota, Primary production in polar waters: Relation to nutrient availability. *Polar Res.* **10**, 87–104 (1991).
78. M. I. O'Connor, J. F. Bruno, S. D. Gaines, B. S. Halpern, S. E. Lester, B. P. Kinlan, J. M. Weiss, Temperature control of larval dispersal and the implications for marine ecology, evolution, and conservation. *Proc. Natl. Acad. Sci.* **104**, 1266–1271 (2007).
79. J. A. Fernandes, W. W. L. Cheung, S. Jennings, Modelling the effects of climate change on the distribution and production of marine fishes: Accounting for trophic interactions in a dynamic bioclimate envelope model. *Glob. Chang. Biol.* **19**, 2596–2607 (2013).
80. N. A. Rayner, P. Brohan, D. E. Parker, C. K. Folland, J. J. Kennedy, M. Vanicek, T. Ansell, S. F. B. Tett, Improved analyses of changes and uncertainties in sea surface temperature measured in situ since the mid-nineteenth century: The HadSST2 Dataset. *J. Clim.* **19**, 446–469 (2006).
81. S. Schlunegger, K. B. Rodgers, J. L. Sarmiento, T. Ilyina, J. P. Dunne, Y. Takano, J. R. Christian, M. C. Long, T. L. Frölicher, R. Slater, F. Lehner, Time of emergence and large ensemble intercomparison for ocean biogeochemical trends. *Glob. Biogeochem. Cycles* **34**, e2019GB006453 (2020).
82. W. W. L. Cheung, R. D. Brodeur, T. A. Okey, D. Pauly, Projecting future changes in distributions of pelagic fish species of Northeast Pacific shelf seas. *Prog. Oceanogr.* **130**, 19–31 (2015).